doi: 10.18323/2782-4039-2023-4-66-8

The influence of addition of ZrO_2 nanoparticles to the electrolyte on the structure and anticorrosion properties of oxide layers formed by plasma electrolytic oxidation on the $Mg_{97}Y_2Zn_1$ alloy

Alisa O. Polunina*[1], researcher of the Research Institute of Advanced Technologies
Anton V. Polunin[2], PhD (Engineering), leading researcher of the Research Institute of Advanced Technologies
Mikhail M. Krishtal[3], Doctor of Sciences (Physics and Mathematics), Professor,
chief researcher of the Research Institute of Advanced Technologies
Togliatti State University, Togliatti (Russia)

***E-mail: a.cheretaeva@tltsu.ru,
alice_raduga@mail.ru**

[1]ORCID: https://orcid.org/0000-0002-3952-9556
[2]ORCID: https://orcid.org/0000-0001-8484-2456
[3]ORCID: https://orcid.org/0000-0001-7189-0002

Received 26.06.2023 *Accepted 27.10.2023*

Abstract: Magnesium alloys with a strengthening long-period stacking ordered structure (LPSO-phase) offer outstanding mechanical properties, but their low corrosion resistance necessitates additional surface protection. The work investigates the influence of adding ZrO_2 nanoparticles at a concentration of 1–4 g/l to the electrolyte on the thickness, structure, composition, wettability, and anticorrosion properties of oxide layers formed during plasma electrolytic oxidation (PEO) of the $Mg_{97}Y_2Zn_1$ alloy with the LPSO-phase. It was found that during PEO, under the influence of an electric field, ZrO_2 nanoparticles penetrate into the forming oxide layer and reduce its porosity. The study revealed a decrease in the quantity and size of pores near the barrier layer in places where the alloy LPSO-phase comes out to the interface with the oxide layer. Low concentrations of ZrO_2 nanoparticles (1–2 g/l) reduce the corrosion rate of the alloy up to two times compared to the base case. The minimum corrosion current density i_{corr}≈14 nA/cm^2 and the highest polarization resistance R_p≈2.6 MΩ·cm^2 are found in the sample formed in an electrolyte with the addition of 1 g/l of ZrO_2 nanoparticles. Calculation of the barrier zone parameters of oxide layers showed that an increase in the ZrO_2 concentration in the electrolyte leads to an increase in the barrier layer thickness and in its specific conductivity, which negatively affects the corrosion resistance of the formed oxide layers – the barrier zone resistance of the layer obtained by adding 4 g/l of ZrO_2, drops by ~20 % compared to the base case (up to ~1 MΩ·cm^2).

Keywords: magnesium alloy; $Mg_{97}Y_2Zn_1$; ZrO_2 nanoparticles; LPSO-phase; plasma electrolytic oxidation; nanoparticles; zirconium oxide; surface contact (wetting) angle; corrosion resistance; barrier zone conductivity.

Acknowledgments: The work was supported by the Russian Science Foundation (Project No. 21-19-00656, https://rscf.ru/project/21-19-00656/).

The paper was written on the reports of the participants of the XI International School of Physical Materials Science (SPM-2023), Togliatti, September 11–15, 2023.

For citation: Polunina A.O., Polunin A.V., Krishtal M.M. The influence of addition of ZrO_2 nanoparticles to the electrolyte on the structure and anticorrosion properties of oxide layers formed by plasma electrolytic oxidation on the $Mg_{97}Y_2Zn_1$ alloy. *Frontier Materials & Technologies*, 2023, no. 4, pp. 87–98. DOI: 10.18323/2782-4039-2023-4-66-8.

INTRODUCTION

Magnesium alloys (MA) belong to the most promising materials for technical and biomedical purposes due to their high specific strength, ability to absorb vibrations and block electromagnetic waves [1–3], as well as complete biocompatibility and biodegradability in the human body [4].

In the last decade, a significant progress has been achieved in the development of MA with an LPSO-structure (long-period stacking-ordered structure, LPSO-phase) [5; 6] with the ultimate strength and ductility comparable to the mechanical characteristics of aluminum alloys and structural steels [7]. However, the formation of an LPSO-structure in MA, as a rule, negatively affects their corrosion resistance due to the resulting potential difference between α-Mg and the strengthening LPSO-phase (up to 200–250 mV), which provokes alloy degradation contacting with a corrosive environment as a result of micro-galvanic corrosion [8; 9]. Therefore, for such alloys it is necessary to provide additional technological solutions to increase their anticorrosion properties.

A promising method for MA surface hardening is micro-arc or plasma electrolytic oxidation (MAO or PEO), which allows forming the protective ceramic layers with high hardness, adhesive strength, wear resistance, and anticorrosion properties [10]. However, the presence of a strengthening LPSO-phase in the alloy complicates micro-arc breakdown and leads to disruption of the barrier layer continuity in places where this phase reaches the "alloy – oxide layer" interface, which reduces the quality and properties of oxide layers obtained in traditional PEO modes [9]. In [9], it was found that treatment of the $Mg_{97}Y_2Zn_1$ alloy in an aluminate electrolyte at an increased frequency of forming pulses (500 Hz) allows forming the most uniform and high-quality oxide layers with high short-term corrosion resistance (impedance modulus is $|Z|_{f=0.01\ Hz}$≈2.2 MΩ·cm^2). However, after a day

of exposure to a corrosive environment, their resistance decreases by 1–2 orders of magnitude.

It is known that the introduction of micro- or nanosized particles (MPs or NPs) of simple SiO_2, ZrO_2, CeO_2, TiO_2, etc. oxides into the electrolyte, as a rule, leads to an increase in the PEO productivity and positively affects the quality and protective properties of oxide layers on magnesium alloys [11; 12]. In [13], a significant increase in the anticorrosion properties of oxide layers was revealed caused by the effect of sealing pores, and blocking access of the corrosive environment to the substrate. It was concluded in [14] that the introduction of ZrO_2 and SiO_2 NPs during PEO leads to an increase in the non-porous layer thickness, as evidenced by a decrease in the constant phase element (CPE_2). It was shown in [2] that a low concentration of NPs (2 g/l) positively affects the oxide layer microstructure, blocking pores and cracks, which gives significant anticorrosion resistance to the coating.

There are very few works on PEO of MAs with the LPSO-phase in Russian and foreign literature [15], and there is no experience in treatment these alloys after adding dispersed particles to the electrolyte. It was possible to find only one work [16], where the authors revealed a significant positive effect from the post-treatment of the oxide layer in a Ce-containing electrolyte on an LPSO alloy, however, this treatment was also carried out in solutions without a dispersed phase. The influence of nanoparticles on the PEO of LPSO alloys in highly-dispersive systems has been practically not studied and is of significant scientific and practical interest. To further improve the protective properties of oxide layers, and increase their long-term anticorrosion characteristics, there is a promising approach based on combining high-frequency PEO [17] and adding insoluble nanosized ZrO_2 particles to the electrolyte, since this substance has proven itself positively in PEO of magnesium alloys [14; 18].

The goal of this research is to study the influence of ZrO_2 nanoparticles, added to the electrolyte during plasma electrolytic oxidation of the $Mg_{97}Y_2Zn_1$ alloy, with the LPSO-phase on the structure, composition, and anticorrosion properties of the formed oxide layers.

METHODS

Samples of oxide layers were obtained on the $Mg_{97}Y_2Zn_1$ magnesium alloy (Solikamsk Experimental-Metallurgical Plant, Solikamsk, Russia), the chemical composition of which was determined on a Thermo Fisher Scientific ARL 4460 OES optical emission spectrometer (Table 1). The basis of the alloy is α-Mg, as well as the $Mg_{12}YZn$ (LPSO-phase) and $Mg_3Zn_3Y_2$ (eutectic phase) phases.

The alloy ingots were preliminary subjected to heat treatment according to the T61 mode: homogenising annealing (525±5 °C, 24 h), quenching in water, and subsequent ageing (200±5 °C, 100 h). Then blanks for PEO were produced in the form of flat parallelepipeds, with a size of 60×20×6 mm^3 and a roughness of $R_a \approx 1$ μm.

Plasma electrolytic oxidation was carried out using alternating current from a power source of own design in a step mode for 10 min. PEO included 3 stages: stage I – "pre-anodising", with anodic forming pulses at a current density of 3 A/dm^2 for 60 s; stage II – increasing (in 10 s), the current density j (RMS) up to 6 A/dm^2 with simultaneous activation of the supply of cathode pulses, at the ratio of currents in the cathode and anode half-periods j_K/j_A=0.5±0.02, and maintaining the mode for 110 s; stage III – increasing j (RMS) up to 7.5 A/dm^2 at j_K/j_A=0.5 and oxidation for 420 s.

At all PEO stages, the pulse frequency f was 1000 Hz, the duty cycle was 50 %, the ratio of the duration of the anodic and cathodic pulse half-periods was 50/50 %, and the ratio of the duration of pauses between half-periods was 50/50 %.

An aqueous solution of potassium hydroxide KOH (1 g/l), sodium phosphate dibasic dodecahydrate $Na_2HPO_4 \times 12H_2O$ (10 g/l), sodium fluoride NaF (10 g/l), and sodium aluminate $NaAlO_2$ (15 g/l) were used as the base electrolyte. During the treatment, continuous circulation and stirring of the electrolyte was ensured at a constant temperature of (14±1) °C. Nanoparticles of crystalline (monoclinic system with a space group of symmetry P21/a) zirconium dioxide ZrO_2 (Plasmotherm Nanopowders, Moscow, Russia), with a dispersion of 40–75 nm at a concentration of 1, 2, 3 or 4 g/l were added to the base electrolyte. The samples of oxide layers obtained in the base electrolyte, as well as in the electrolyte with additions of ZrO_2 nanoparticles, are further marked as *B*, *Z*1, *Z*2, *Z*3, and *Z*4, respectively.

Structural studies of oxide layers were carried out on transverse metallographic sections, using a Carl Zeiss field-emission scanning electron microscope (SEM) in the backscattered electron mode. The elemental (chemical) composition of the oxide layers was determined by energy dispersive X-ray microanalysis (EDX, EDAX TEAM EDS analyzer based on SDD Apollo X Sigma SEM). To eliminate polarisation effects during SEM studies, a conductive *Pt* layer was preliminarily applied to the sections using cold magnetron sputtering. The thickness (T, μm) and porosity (P, %) of the oxide layers were estimated from three panoramic cross-sectional images (≥500 μm in length) using ImageJ software.

Table 1. *Chemical composition of the $Mg_{97}Y_2Zn_1$ alloy*
Таблица 1. *Химический состав сплава $Mg_{97}Y_2Zn_1$*

Element	Mg	Y	Zn	Zr	Nd	Mn
Content, wt. %	89.90±0.15	6.67±0.17	2.27±0.10	1.07±0.26	0.056±0.001	<0.005

Note. ±3σ is given as an error. Al and Fe content is <0.002 wt. %.
Примечание. В качестве погрешности приведено ±3σ. Содержание Al и Fe <0,002 мас. %.

The wettability (degree of hydrophobicity/hydrophilicity) of the surface of the oxide layers, was assessed by the sessile drop method using a KRUSS DSA-25E contact angle analyser (Germany) with an automatic precision dosing system. Drop volume – 3 μl, application speed – 1 μl/s. Wetting (contact) liquid – 3.5 wt. % NaCl solution.

Electrochemical tests were carried out by potentiodynamic polarisation and impedance spectroscopy using a SmartStat PS-50 potentiostat-galvanostat (Electrochemical Instruments, Russia) with a built-in module for measuring electrochemical impedance of 3.5 wt. % NaCl (295±2 K), in a three-electrode electrochemical cell CS936 (CorrTest, China) with a fixed contact area of 1 cm^2. A platinum grid (20×20 mm^2) served as an auxiliary electrode; a silver chloride electrode filled with a saturated potassium chloride solution ($Ag/AgCl/KCl_{sat}$) was used as a reference electrode. Stabilisation of the electrode potential of the samples (E_{oc} – open circuit potential, V) was carried out for 60 min. Potentiodynamic polarisation of the samples was carried out in the range from −150 mV to +1000 mV relative to E_{oc} with a potential scanning rate of 1 mV/s. The polarisation resistance R_p was determined according to the recommendations of ASTM G102-89(2015)e1 using the Stern–Geary constant. The effective interconnected porosity (P_{eff}, %) of the oxide layers was assessed using the electrochemical method in a similar way [19].

Measurements using the electrochemical impedance spectroscopy (EIS) method were carried out with a sinusoidal disturbing signal, with an amplitude of 10 mV at a stabilised E_{oc} value, in the frequency range from 500 kHz to 10 mHz. Analysis of experimental data and calculation of parameters of equivalent circuits, were carried out using ZView software (Scribner Associates, USA). The barrier zone parameters (thickness and conductivity) were determined from data on processing impedance spectra in a similar way [20].

RESULTS

Structure and chemical (elemental) composition of oxide layers

The base oxide layer *B* formed in the electrolyte without NP additives contains multiple transverse pores and cracks, which can reach almost the barrier layer or magnesium substrate (Fig. 1 a). A large number of closed pores formed as a result of a sharp discharge of hot gases, from the layer formation zone are observed, and the internal (barrier) layer at the "oxide layer – magnesium alloy" interface has a pronounced mesoporous structure and discontinuities, and has discontinuities in the areas of LPSO-phase release to the surface (Fig. 1 b).

The introduction of ZrO_2 NPs into the electrolyte, leads to the formation of oxide layers with a more uniform structure, their porosity in the cross section decreases from ~9 % to ~5.5–7 %, the length and number of voids and pores near the barrier layer, and at the points of LPSO-phase, exit to the interface with the magnesium substrate are reduced (Fig. 1 c–f). In this case, a semblance of a bordering with a changed phase contrast appears above the LPSO-phase, which indicates the oxidation of this phase along the perimeter, and the barrier layer formation in places where it reaches the "oxide layer – magnesium alloy" interface.

In the images of the structure of the *Z*1–*Z*4 oxide layers, multiple bright points and globules, with sizes ranging from a fraction of a micron to 5–10 μm, with a sharp phase contrast are observed (Fig. 1 c–f), which indicates the presence of heavy elements in them, and taking into account the experimental factor, allows stating that these are embedded ZrO_2 NPs or products of their reactions, with other components of the system. An increase in the proportion of Zr from ~6.9 % for the base sample to ~9.3 wt. % for the sample produced by adding 4 g/l ZrO_2 to the electrolyte, indicates the successful inclusion of nanoparticle substance into the layer (EDX analysis data, Table 2). Zirconium replaces predominantly F and Na in the layer, and the content of other elements remains virtually unchanged (Table 2).

The addition of ZrO_2 NPs had virtually no effect on the PEO efficiency – an increase in the average oxide layer thickness from ~22 to ~26 μm is observed only in the case of a low concentration of the dispersed phase in the electrolyte (sample *Z*1), while the average thickness of the *Z*2–*Z*4 oxide layers is at the base layer level and is ~20–22 μm (Fig. 1).

Wettability and anticorrosion properties of oxide layers

The addition of ZrO_2 nanoparticles to the electrolyte changes the surface contact properties of the formed oxide layers – the surface contact (wetting) angle Θ of *Z*1–*Z*4 samples is 95–115° versus ~91° for the base oxide layer, i. e., it is increased by 5–20 %, which indicates an increase in the hydrophobicity of the *Z*1–*Z*4 oxide layers (Fig. 2). Moreover, over time (10 min), the change in the contact (wetting) angle for samples *Z*1–*Z*4 is significantly less (less than 20°) than for the base oxide layer, which indirectly indicates a lower open porosity of the oxide layers, as well as a more developed surface microrelief.

Fig. 3 shows the polarisation curves of the samples under study in the logarithmic scale of current density. The original $Mg_{97}Y_2Zn_1$ alloy (without an oxide layer) has a relatively low corrosion resistance (i_{corr}≈5 μA/cm^2, R_p≈8 kΩ·cm^2) and is prone to pitting corrosion in chloride-containing environments (Fig. 3, Table 3). MA PEO in the base electrolyte reduces the corrosion rate of the alloy by more than 2 orders of magnitude – to i_{corr}≈26 nA/cm^2 and R_p≈1.6 MΩ·cm^2.

The addition of ZrO_2 nanoparticles at a concentration of 1–2 g/l leads to a decrease in the average values of i_{corr} by ~1.5–2 times (up to 14–17 nA/cm^2), and an increase in R_p from ≈1.6 MΩ·cm^2 for the base layer to ≈2.6 and 2.3 MΩ·cm^2 for samples *Z*1 and *Z*2, respectively, as well as to a decrease in the effective interconnected porosity P_{eff} up to 0.009 % and 0.013 % for these samples versus 0.019 % for the base oxide layer (Table 3). However, at a higher polarising voltage (+1 V), this effect is leveled out, and the anodic current densities of both the base sample and samples *Z*1–*Z*4 almost reach the current density of the alloy without an oxide layer (Fig. 3, Table 3). An increase in the concentration of ZrO_2 NPs in the electrolyte to 3–4 g/l worsens the anticorrosion properties of the layers to the level of the base layer *B* with a slight decrease in P_{eff} from ≈0.19 % to 0.14–0.17 % (Table 3).

The Nyquist (Fig. 4 a) and Bode plots (Fig. 4 b), which make it possible to determine the electrical parameters of the "alloy – electrolyte" interface, show that a protective

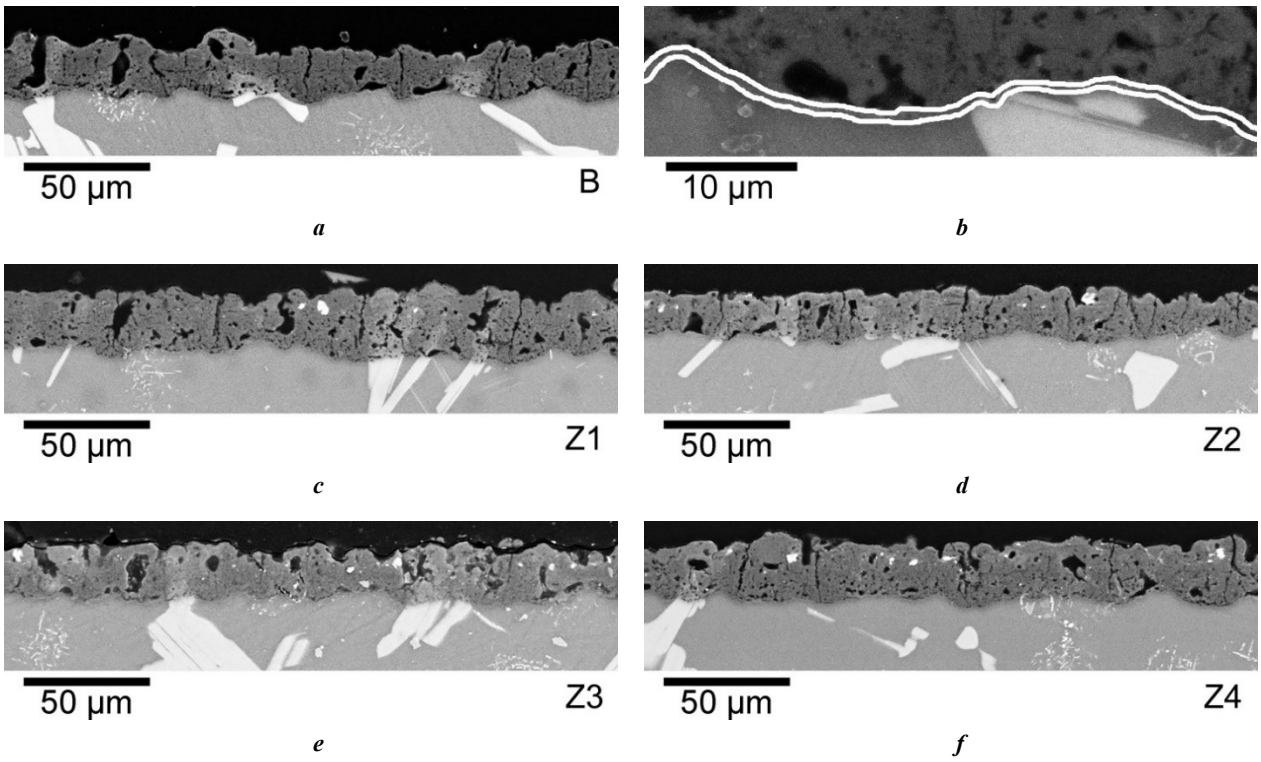

Fig. 1. *Microstructures (cross sections, SEM) of the base (B) oxide layer (panoramic view (**a**) and detailing of the barrier zone (**b**)) and the oxide layers produced when adding ZrO_2 nanoparticles to the electrolyte (Z1–Z4): 1 g/l (**c**), 2 g/l (**d**), 3 g/l (**e**), 4 g/l (**f**)*

Рис. 1. *Микроструктура (поперечные сечения, СЭМ) базового (B) оксидного слоя (панорамный снимок (**a**) и детализация барьерной зоны (**b**)) и оксидных слоев, полученных при добавлении в электролит наночастиц ZrO_2 (Z1–Z4): 1 г/л (**c**), 2 г/л (**d**), 3 г/л (**e**), 4 г/л (**f**)*

Table 2. *Chemical (elemental) composition of oxide layers (EDX, wt. %)*

Таблица 2. *Химический (элементный) состав оксидных слоев (EDX, мас. %)*

Sample	Mg	O	Al	F	Na	P	Y	Zr
B	31.9±2.2	29.9±0.4	15.2±1.3	7.3±0.7	2.3±1.1	2.1±0.4	3.6±1.4	6.9±0.8
***Z*1**	32.6±1.0	29.7±0.6	16.3±1.0	6.5±1.2	1.3±0.7	2.4±0.5	3.3±1.0	7.4±0.6
***Z*2**	31.8±1.9	29.7±0.9	15.6±0.9	6.6±0.8	1.9±0.7	2.1±0.4	3.6±1.9	8.0±0.5
***Z*3**	30.1±1.6	30.8±0.3	15.7±1.0	5.5±0.8	1.4±0.8	2.4±0.3	4.5±1.6	9.1±0.8
***Z*4**	32.1±1.5	29.7±0.5	15.7±1.0	6.4±0.7	2.0±0.3	2.1±0.3	2.7±0.3	9.3±0.6

Note. ±3σ is given as an error.

Примечание. В качестве погрешности приведено ±3σ.

passivating film is formed on the non-oxidised $Mg_{97}Y_2Zn_1$ alloy after 60 min of exposure to a corrosive environment, the best description of which is achieved in the case of using a simple equivalent circuit, with one *R*–*C* chain (Fig. 4 c) simulating the double-layer capacitance, and the resistance of charge transfer across the interface.

The spectra of samples with oxide layers have two extrema in the phase angle graph (Fig. 4 b), therefore, to process them, a double-loop circuit was used, which corresponds to two time constants (Fig. 4 d). The first inflection in the high-frequency range is determined by the presence of an outer porous layer R_{out}, and the second one (in the range of medium and low frequencies) characterises the inner barrier zone R_b.

PEO allowed increasing significantly the corrosion resistance of the $Mg_{97}Y_2Zn_1$ alloy – the charge transfer resistance of the barrier zone R_b of the base oxide layer was ≈1.3 MΩ cm^2 versus ≈0.9 kΩ cm^2 for the natural passive film on the alloy, i. e., by more than 3 orders of magnitude (Fig. 4, Table 4). The addition of ZrO_2 NPs introduced into the electrolyte in concentrations of 1–2 g/l increased R_b of the oxide layers up to ≈1.8 and 1.6 MΩ·cm^2, respectively,

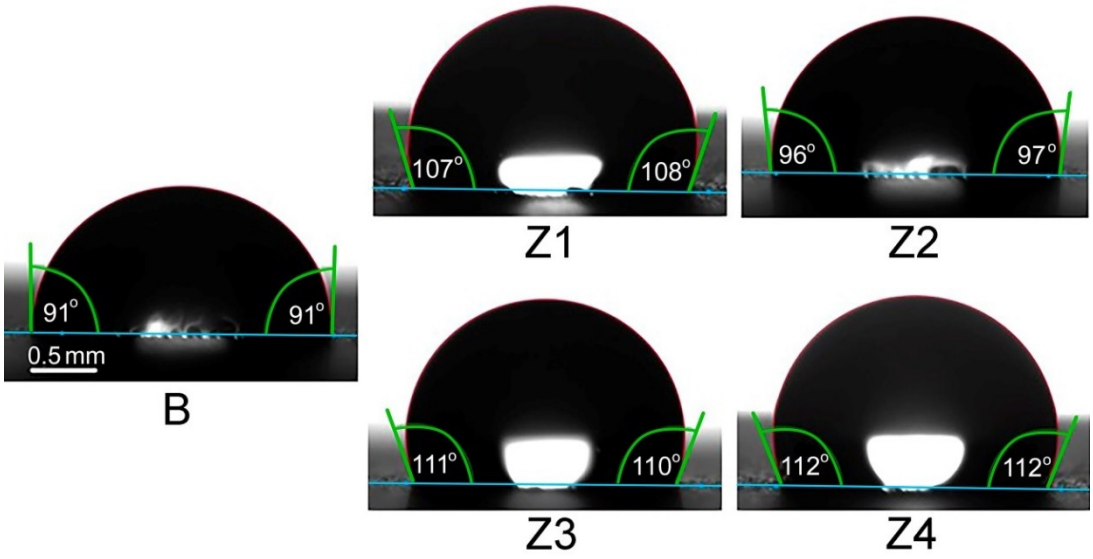

Fig. 2. *Wettability of the surface of oxide layers formed in the base electrolyte (B) and with additions of ZrO_2 NPs from 1 to 4 g/l (Z1, Z2, Z3, Z4). Contact medium is 3.5 wt. % NaCl*
Рис. 2. *Смачиваемость оксидных слоев, сформированных в базовом электролите (B) и с добавками НЧ ZrO_2 от 1 до 4 г/л (Z1, Z2, Z3, Z4). Контактная среда – 3,5 мас. % NaCl*

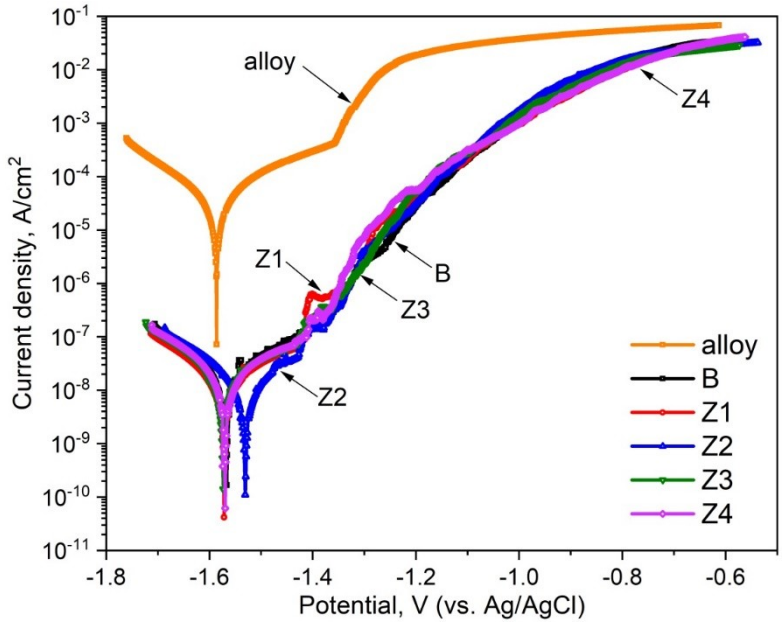

Fig. 3. *Polarization curves of samples from the $Mg_{97}Y_2Zn_1$ alloy in the initial state and with oxide layers formed in the base electrolyte (B) and with additions of ZrO_2 NPs from 1 to 4 g/l (Z1, Z2, Z3, Z4)*
Рис. 3. *Поляризационные кривые образцов из сплава $Mg_{97}Y_2Zn_1$ в исходном состоянии и с оксидными слоями, сформированными в базовом электролите (B) и с добавками НЧ ZrO_2 от 1 до 4 г/л (Z1, Z2, Z3, Z4)*

i. e. by ~30 and ~15 % compared to the base oxide layer. However, a further increase in the ZrO_2 concentration in the electrolyte (especially 4 g/l) led to a decrease in the protective properties of the oxide layers to the level of the base oxide layer (Fig. 4, Table 4).

The main studied characteristics of the oxide layers, determining their properties were divided into two groups (Table 5). The first group (thickness T, structural (visual) porosity P, and surface wettability Θ) refers to the characteristics of the outer (porous) zone of the layer. The second group (the barrier zone thickness T_b, effective interconnected porosity P_{eff}, and specific conductivity σ_b) characterises mainly the parameters of the inner barrier zone, of the oxide layer at the interface with the alloy.

Table 3. *The results of polarization tests of the $Mg_{97}Y_2Zn_1$ alloy before and after PEO in the base electrolyte and with additions of ZrO_2 NPs (3.5 wt. % NaCl)*
Таблица 3. *Результаты поляризационных испытаний сплава $Mg_{97}Y_2Zn_1$ до и после ПЭО в базовом электролите и с добавками НЧ ZrO_2 (3,5 мас. % NaCl)*

Sample	E_{oc}, V	I_{corr}, nA/cm^2	E_{corr}, V	R_p, MΩ·cm^2	P_{eff}, %
Alloy	−1.584±0.028	4600±3641	−1.470±0.028	0.008±0.004	–
B	−1.528±0.020	25.7±11.5	−1.540±0.019	1.56±0.80	0.19±0.04
***Z*1**	−1.537±0.027	13.7±1.7	−1.558±0.018	2.58±0.50	0.09±0.01
***Z*2**	−1.527±0.027	17.3±2.1	−1.541±0.036	2.28±0.73	0.13±0.02
***Z*3**	−1.557±0.012	22.0±0.6	−1.556±0.034	1.68±0.61	0.14±0.02
***Z*4**	−1.566±0.022	25.8±9.9	−1.580±0.014	1.67±0.50	0.17±0.03

Note. E_{oc} *is open circuit potential;* i_{corr} *is corrosion current density;* E_{corr} *is corrosion potential;* R_p *is polarisation resistance;* P_{eff} *is effective interconnected porosity.*
Примечание. E_{oc} *– потенциал разомкнутой цепи;* i_{corr} *– плотность тока коррозии;* E_{corr} *– потенциал коррозии;* R_p *– поляризационное сопротивление;* P_{eff} *– эффективная сквозная пористость.*

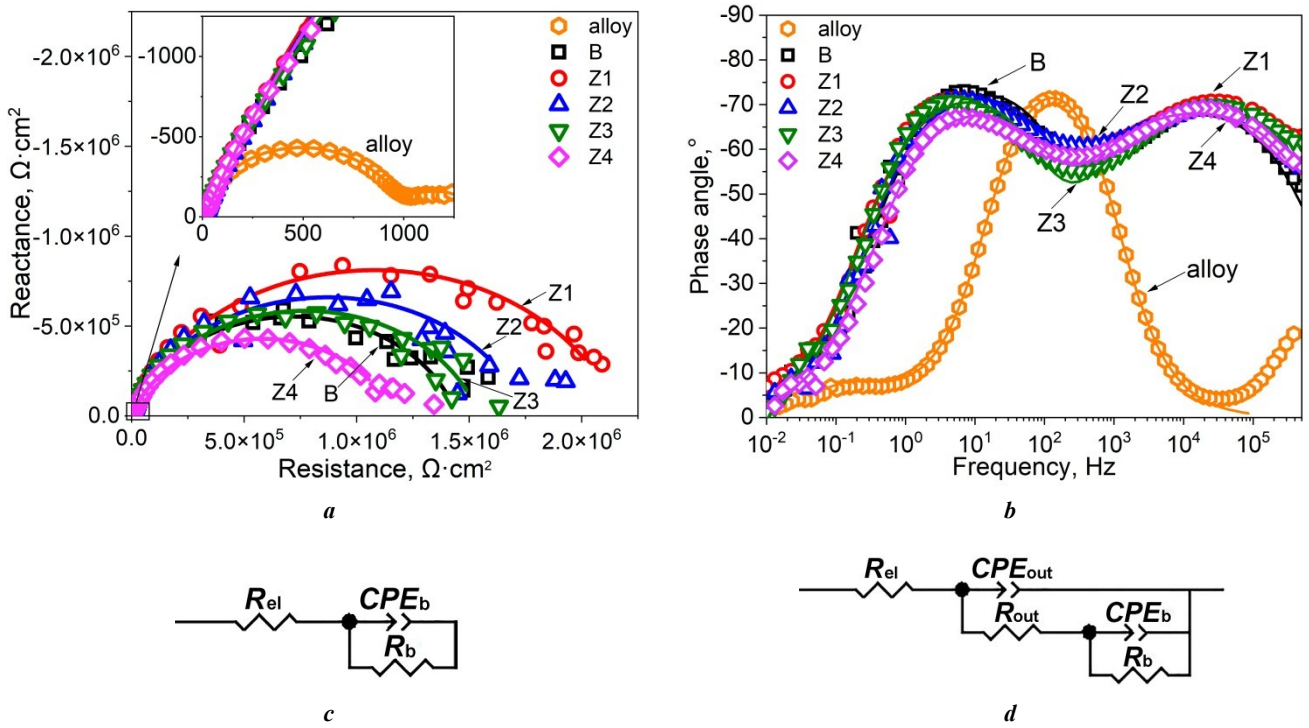

Fig. 4. *Nyquist (**a**) and Bode (**b**) plots of $Mg_{97}Y_2Zn_1$ alloy samples without coating (insert) and with oxide layers formed in the base electrolyte (B) and with additions of ZrO_2 NPs from 1 to 4 g/l (Z1, Z2, Z3, Z4). Equivalent electrical circuits used to describe the impedance spectra of uncoated alloy (**c**) and samples of alloy with oxide layers (**d**)*
Рис. 4. *Кривые Найквиста (**a**) и Боде (**b**) образцов из сплава $Mg_{97}Y_2Zn_1$ без покрытия (вставка) и с оксидными слоями, сформированными в базовом электролите (B) и с добавками НЧ ZrO_2 от 1 до 4 г/л (Z1, Z2, Z3, Z4). Эквивалентные электрические схемы, используемые для описания спектров импеданса образцов из сплава без покрытия (**c**) и с оксидными слоями (**d**)*

Table 4. *The results of processing EIS data of the $Mg_{97}Y_2Zn_1$ alloy before and after PEO in the base electrolyte and with additions of ZrO_2 nanoparticles (3.5 wt. % NaCl)*
Таблица 4. *Результаты обработки данных ЭИС сплава $Mg_{97}Y_2Zn_1$ до и после ПЭО в базовом электролите и с добавками наночастиц ZrO_2 (3,5 мас. % NaCl)*

Sample	R_{out}, kΩ·cm^2	CPE_{out}		R_b, MΩ·cm^2	CPE_b	
		Q_{out}, $\Omega^{-1}\cdot cm^{-2}\cdot s^n$	n_{out}		Q_b, $\Omega^{-1}\cdot cm^{-2}\cdot s^n$	n_b
Alloy	–	–	–	$(1\pm0.3)\cdot10^{-3}$	$(1.6\pm0.1)\cdot10^{-5}$	0.94±0.01
B	10.5±0.6	$(3.0\pm0.3)\cdot10^{-7}$	0.79±0.01	1.27±0.30	$(1.5\pm0.2)\cdot10^{-7}$	0.91±0.03
***Z*1**	13.7±2.3	$(2.8\pm0.3)\cdot10^{-7}$	0.79±0.01	2.14±1.04	$(1.6\pm0.2)\cdot10^{-7}$	0.88±0.01
***Z*2**	11.6±4.9	$(3.0\pm0.2)\cdot10^{-7}$	0.79±0.01	1.74±0.96	$(1.7\pm0.5)\cdot10^{-7}$	0.88±0.03
***Z*3**	11.0±2.7	$(3.1\pm0.3)\cdot10^{-7}$	0.78±0.01	1.53±0.50	$(2.8\pm0.7)\cdot10^{-7}$	0.86±0.04
***Z*4**	13.5±2.7	$(2.9\pm0.1)\cdot10^{-7}$	0.79±0.01	1.01±0.24	$(2.2\pm0.5)\cdot10^{-7}$	0.84±0.03

*Note. R_{out} and R_b are the resistances of the outer and barrier zones of the oxide layer; CPE_{out} and CPE_b are the constant phase elements characterizing the capacitance of the outer (porous) and inner (barrier) zones, taking into account the degree of their heterogeneity; **Q** is a frequency-independent parameter; **n** is an exponential factor (n≤1).*
*Примечание. R_{out} и R_b – сопротивление внешней и барьерной зон оксидного слоя; CPE_{out} и CPE_b – элементы постоянной фазы, характеризующие емкость внешней (пористой) и внутренней (барьерной) зон с учетом степени их гетерогенности; **Q** – частотно-независимый параметр; **n** – экспоненциальный фактор (n≤1).*

Table 5. *Characteristics of zones of oxide layers*
Таблица 5. *Характеристики зон оксидных слоев*

Sample	Outer layer			Barrier layer		
	***T*, μm**	***P*, %**	**Θ, °**	T_b, nm	P_{eff}, %	σ_b, pS/cm
B	21.9±2.5	8.8±0.5	91.2±1.3	215±78	0.19±0.04	12.3±1.6
***Z*1**	25.8±3.1	7.7±0.1	107.5±2.6	307±97	0.09±0.01	18.7±2.6
***Z*2**	19.1±4.2	5.4±0.2	96.6±1.9	274±62	0.13±0.02	20.3±7.2
***Z*3**	21.7±3.3	6.7±0.1	110.4±2.1	250±111	0.14±0.02	23.2±5.2
***Z*4**	22.1±4.3	5.6±0.9	111.9±2.8	382±96	0.17±0.03	33.8±8.4

*Note. **T** is oxide layer thickness; **P** is structural porosity; **Θ** is contact angle of surface wettability; T_b is barrier zone thickness; P_{eff} is effective interconnected porosity; σ_b is barrier layer conductivity.*
*Примечание. **T** – толщина оксидного слоя; **P** – структурная пористость; **Θ** – краевой угол смачиваемости поверхности; T_b – толщина барьерной зоны; P_{eff} – эффективная сквозная пористость; σ_b – удельная проводимость барьерного слоя.*

DISCUSSION

The results of the study of the chemical (elemental) composition showed the inclusion of ZrO_2 NPs in the formed oxide layer, and with an increase in the dispersed additive concentration in the electrolyte by 1 g/l, the Zr proportion in the layer increases by ≈0.5–1 wt. %. One can assume that the introduction of ZrO_2 particles occurs both in the original (nanosized) and agglomerated form. The particles were detected mainly in the upper zones of the layers (30–50 % of the coating thickness), and have a clearly defined contrast boundary with the oxide layer material, which indicates their inclusion as a result of being captured by a molten metal splash with subsequent fixation in the layer. The absence of transition colour zones in the phase contrast, as well as the phase contrast heterogeneity in the zones of inclusion of ZrO_2 particles in the layer, and the light areas themselves, indirectly indicates the inclusion of ZrO_2 NPs exactly in the form of particles without participation in chemical reactions, and the formation of Zr-containing phases. The presence of zirconium in the base layer (Table 2), as well as characteristic contrasting (light)

zones in the images of the transverse structure (Fig. 1 a), indicates the effect of the oxide layer inheriting the structure, and chemical heterogeneity of the processed alloy, which was previously revealed during PEO of aluminum-silicon alloys [21].

The inclusion of ZrO_2 NPs in agglomerated micro- and nanosized form into the oxide layer, and in particular, into its surface is also evidenced by data on the wettability of oxide layers (Fig. 2). It is known that with a decrease in the radius of the surface morphological element that comes into contact with the liquid, the necessary external pressure to ensure surface wettability (Laplace formula), sharply increases [22]. And at constant external pressure, the contact liquid cannot go around and wet objects with a certain critical *R* due to the surface tension in the liquid. A change in the contact wetting angle (Fig. 2, Table 5), suggests that, along with a change in the effective interconnected porosity of the oxide layers, there is an increase in the surface microrelief development, due to the introduction of ZrO_2 particles into it, which creates numerous micro- and nano-objects that cannot be wetted with contact fluid at atmospheric external pressure. As a consequence, as a result of microscopic effects, macroscopic changes in contact wetting angles are observed in terms of increasing the hydrophobicity of the oxide layers. Due to the effects of charge accumulation on the oxide layer surface, and as a consequence, the appearance of polarisation artifacts in microscopic areas of the sample, we were unable to resolve and visualise individual ZrO_2 nanoparticles embedded in the layer using the SEM method, therefore, this will be the subject of further research using the method of atomic force microscopy, and optical profilometry based on white light interferometry.

The influence of ZrO_2 NPs on the oxide layer structure, and most importantly, the structure and quality of its barrier zone, is evidenced as well by the EIS measurement data. It is known that oxide layers, formed by PEO have a two- and/or three-zone structure [17; 23]. The outer (porous) zone of the layer is the primary barrier limiting the contact of the corrosive environment with the alloy surface. The main indicators of high anticorrosion properties of the outer zone, as a rule, are low porosity, as well as surface hydrophobicity, which prevents the penetration of an aggressive environment into the pores and channels of microarc discharges. It is considered that the internal (barrier) zone at the interface with the alloy, makes the main contribution to the anticorrosion properties of oxide layers [24]. It is known that the thickness of the oxide layer barrier zone according to microstructure photographs (SEM) ranges from several tens of nm to several microns. Depending on the anodising or PEO mode [10], however, it is quite difficult to measure this value clearly due to the microscope resolution and polarisation effects (non-conducting layer) [23].

The study showed, that no correlation between the parameters of the outer zone of oxide layers *B*, and *Z*1–*Z*4 with their anticorrosion properties is observed: the inclusion of ZrO_2 NPs in the oxide layers reduces their structural porosity, but does not affect the increase in their protective properties (Fig. 5 a). The corrosion current density of sample *Z*4, which has the lowest porosity ($P \approx 5.6$ %), is higher than that of the base layer, i. e., even the opposite trend is observed. The influence of the hydrophobicity degree, on the anticorrosion properties of oxide layers, was identified only for cases of low concentration of ZrO_2 NPs added to the electrolyte (1–2 g/l). A further increase in the concentration of nanoparticles, despite an increase in the contact (wetting) angle, leads to an increase in the corrosion rate of the alloy (Fig. 5 b).

Despite the increase in the thickness of the inner zone T_b (Table 5) under the influence of the addition of ZrO_2 NPs to the electrolyte, an increase in the Zr concentration in the layer leads to an increase in effective interconnected porosity and an increase in specific conductivity (Table 5). Probably, solid hard ZrO_2 nanoparticles are accelerated in the vapour-gas phase, preceding the microarc discharge breakdown, under the influence of an electric field they break through the oxide layer to the barrier zone and penetrate into it, thereby changing its conductivity

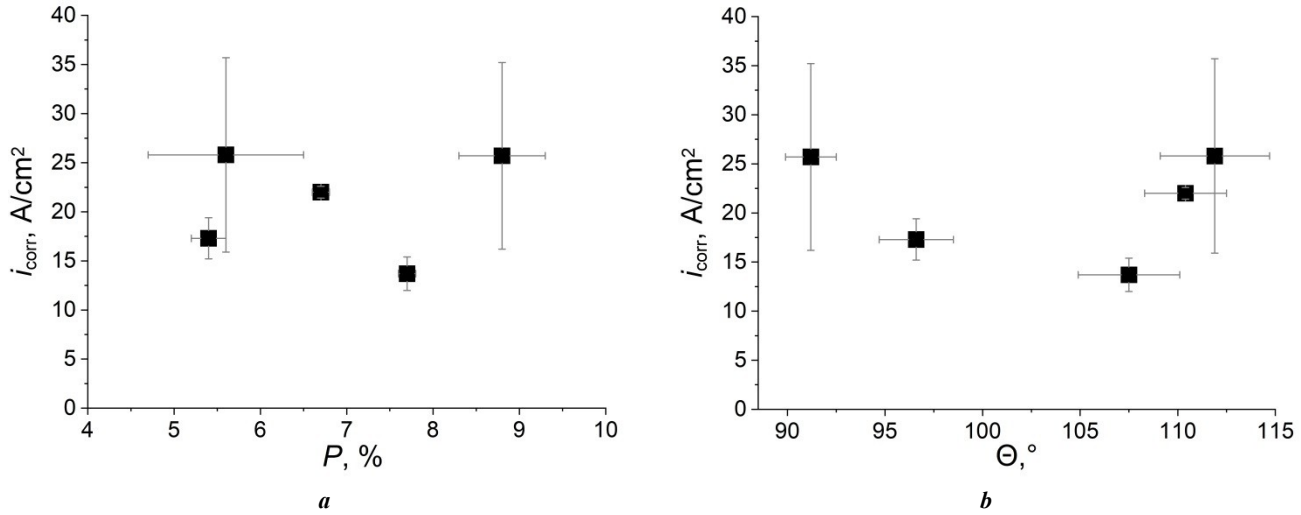

Fig. 5. *Relationship between the corrosion current density of oxide layers and their structural porosity (**a**) and the contact angle of surface wettability (**b**)*

Рис. 5. *Связь плотности тока коррозии оксидных слоев с их структурной пористостью (**a**) и краевым углом смачивания поверхности (**b**)*

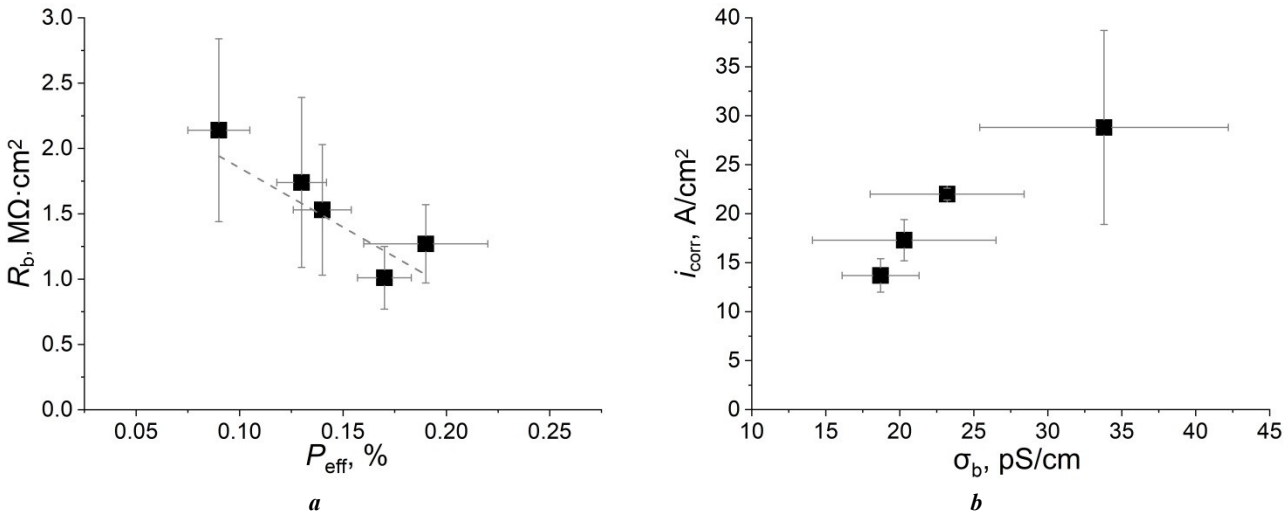

Fig. 6. *Resistance of the barrier zone of oxide layers depending on their effective interconnected porosity* ***(a)*** *and the relationship between the corrosion current density of layers Z1–Z4 and the barrier zone specific conductivity* ***(b)***
Рис. 6. *Сопротивление барьерной зоны оксидных слоев в зависимости от их эффективной сквозной пористости* ***(а)*** *и связь плотности тока коррозии слоев Z1–Z4 с удельной проводимостью барьерной зоны* ***(b)***

(Table 5). Apparently, as a result of the inelastic collision of nanoparticles with a layer, nanosized channels and nanocracks are formed in the barrier layer [25], which reduce the effective thickness of the barrier layer, and in the case of contact with a corrosive environment, reduce its electrical resistance.

With increasing barrier zone conductivity, a sharp decrease in anticorrosion properties is observed: an almost linear decrease in the barrier layer resistance with increasing P_{eff} (Fig. 6 a), as well as a sharp increase in the corrosion rate of the alloy (i_{corr}) (Fig. 6 b) is revealed. Thus, the barrier layer dielectric properties and continuity have a decisive influence on the anticorrosion properties of the oxide layers.

CONCLUSIONS

1. The addition of ZrO_2 nanoparticles to the electrolyte during PEO of the Mg LPSO alloy $Mg_{97}Y_2Zn_1$ at a concentration of 1–2 g/l reduces the porosity of the formed oxide layers, and promotes the oxidation of the LPSO-phase emerging at the "magnesium alloy – oxide layer" interface, as well as the formation of a continuous and dense barrier layer.

2. The addition of ZrO_2 nanoparticles to the electrolyte at a concentration of 1 g/l increases the thickness of the oxide layer by ≈20 %, and increases the oxide layer anticorrosion properties by ~2 times compared to the base version. When the concentration of ZrO_2 NPs in the electrolyte increases to 3–4 g/l, the thickness and protective properties of the oxide layers return to the base level.

3. It was identified that the main parameters influencing the anticorrosion properties of the formed oxide layers, are their effective interconnected porosity P_{eff} and the barrier zone specific conductivity σ_b that increase with increasing ZrO_2 concentration in the electrolyte from 1 to 4 g/l, which negatively affects anticorrosion properties of oxide layers, reducing their complex resistance.

4. It is shown that under the influence of an electric field, solid ZrO_2 nanoparticles, as a result of inelastic collision, break through the oxide layer to the barrier zone and penetrate into it, which changes its thickness and conductivity due to the formation of breakdown channels, and nano- and microcracks, and as a consequence, leads to reducing the oxide layer anticorrosion properties.

REFERENCES

1. Landkof B. Magnesium Applications in Aerospace and Electronic Industries. *Magnesium Alloys and their Applications*, 2006, pp. 168–172. DOI: 10.1002/3527607552.CH28.
2. Ur Rehman Z., Choi Dongjin. Investigation of ZrO_2 nanoparticles concentration and processing time effect on the localized PEO coatings formed on AZ91 alloy. *Journal of Magnesium and Alloys*, 2019, vol. 7, no. 4, pp. 555–565. DOI: 10.1016/J.JMA.2019.10.001.
3. Fattah-alhosseini A., Chaharmahali R., Babaei K., Nouri M., Keshavarz M.K., Kaseem M. A review of effective strides in amelioration of the biocompatibility of PEO coatings on Mg alloys. *Journal of Magnesium and Alloys*, 2022, vol. 10, no. 9, pp. 2354–2383. DOI: 10.1016/J.JMA.2022.09.002.
4. Sedelnikova M.B., Kashin A.D., Uvarkin P.V., Tolmachev A.I., Sharkeev Y.P., Ugodchikova A.V., Lugi-
nin N.A., Bakina O.V. Porous biocoatings based on diatomite with incorporated ZrO_2 particles for biodegradable magnesium implants. *Journal of Functional Biomaterials*, 2023, vol. 14, no. 5, article number 241. DOI: 10.3390/JFB14050241.
5. Xu Daokui, Han En-hau, Xu Yongbo. Effect of long-period stacking ordered phase on microstructure, mechanical property and corrosion resistance of Mg alloys: A review. *Progress in Natural Science: Materials International*, 2016, vol. 26, no. 2, pp. 117–128. DOI: 10.1016/J.PNSC.2016.03.006.
6. Wang Guoxin, Mao Pingli, Wang Zhi, Zhou Le, Wang Feng, Liu Zheng. High strain rates deformation

behavior of an as-extruded Mg-2.5Zn-4Y magnesium alloy containing LPSO phase at high temperatures. *Journal of Materials Research and Technology*, 2022, vol. 21, pp. 40–53. DOI: 10.1016/J.JMRT.2022.08.131.
7. Qian Yafeng, Zhao Yanhui, Dong Xiaorui, Yu Wei, Feng Jianhang, Yu Hui. Microstructure, mechanical properties and fire resistance of high strength Mg-Gd-Y-Zr alloys. *Metals*, 2022, vol. 12, no. 9, article number 1456. DOI: 10.3390/MET12091456.
8. Li C.Q., Xu D.K., Zeng Z.R., Wang B.J., Sheng L.Y., Chen X.B., Han E.H. Effect of volume fraction of LPSO phases on corrosion and mechanical properties of Mg-Zn-Y alloys. *Materials & Design*, 2017, vol. 121, pp. 430–441. DOI: 10.1016/j.matdes.2017.02.078.
9. Cheretaeva A.O., Glukhov P.A., Shafeev M.R., Denisova A.G., Borgardt E.D., Polunin A.V., Katsman A.V., Krishtal M.M. Improvement of protective oxide layers formed by high-frequency plasma electrolytic oxidation on Mg-RE alloy with LPSO-phase. *Chimica Techno Acta*, 2023, vol. 10, no. 2, article number 202310212. DOI: 10.15826/chimtech.2023.10.2.12.
10. Simchen F., Sieber M., Kopp A., Lampke T. Introduction to plasma electrolytic oxidation – an overview of the process and applications. *Coatings*, 2020, vol. 10, no. 7, article number 628. DOI: 10.3390/COATINGS10070628.
11. Lu Xiaopeng, Blawert C., Huang Yuanding, Ovri H., Zheludkevich M.L., Kainer K.U. Plasma electrolytic oxidation coatings on Mg alloy with addition of SiO_2 particles. *Electrochimica Acta*, 2016, vol. 187, pp. 20–33. DOI: 10.1016/J.ELECTACTA.2015.11.033.
12. Mashtalyar D.V., Imshinetskiy I.M., Nadaraia K.V. et al. Effect of TiO_2 nanoparticles on the photocatalytic properties of PEO coatings on Mg alloy. *Journal of Magnesium and Alloys*, 2023, vol. 11, no. 2, pp. 735–752. DOI: 10.1016/J.JMA.2022.10.021.
13. Bordbar-Khiabani A., Yarmand B., Mozafari M. Enhanced corrosion resistance and in-vitro biodegradation of plasma electrolytic oxidation coatings prepared on AZ91 Mg alloy using ZnO nanoparticles-incorporated electrolyte. *Surface and Coatings Technology*, 2019, vol. 360, pp. 153–171. DOI: 10.1016/J.SURFCOAT.2019.01.002.
14. Gnedenkov S.V., Sinebryukhov S.L., Mashtalyar D.V., Imshinetskiy I.M., Samokhin A.V., Tsvetkov Y.V. Fabrication of coatings on the surface of magnesium alloy by plasma electrolytic oxidation using ZrO_2 and SiO_2 Nanoparticles. *Journal of Nanomaterials*, 2015, vol. 2015, article number 154298. DOI: 10.1155/2015/154298.
15. Wu Jiahao, Wu Liang, Yao Wenhui, Chen Yanning, Chen Yonghua, Yuan Yuan, Wang Jingfeng, Atrens A., Pan Fusheng. Effect of electrolyte systems on plasma electrolytic oxidation coatings characteristics on LPSO Mg-Gd-Y-Zn alloy. *Surface and Coatings Technology*, 2023, vol. 454, article number 129192. DOI: 10.1016/J.SURFCOAT.2022.129192.
16. Mohedano M., Pérez P., Matykina E., Pillado B., Garcés G., Arrabal R. PEO coating with Ce-sealing for corrosion protection of LPSO Mg–Y–Zn alloy. *Surface and Coatings Technology*, 2020, vol. 383, article number 125253. DOI: 10.1016/J.SURFCOAT.2019.125253.
17. Liu Xiaohe, Liu Lei, Dong Shuai, Chen Xiao-Bo, Dong Jie. Towards dense corrosion-resistant plasma electrolytic oxidation coating on Mg-Gd-Y-Zr alloy by using ultra-high frequency pulse current. *Surface and Coatings Technology*, 2022, vol. 447, article number 128881. DOI: 10.1016/J.SURFCOAT.2022.128881.
18. Kang Min Lee, Ki Ryong Shin, Seung Namgung, Bongyoung Yoo, Dong Hyuk Shin. Electrochemical response of ZrO_2-incorporated oxide layer on AZ91 Mg alloy processed by plasma electrolytic oxidation. *Surface and Coatings Technology*, 2011, vol. 205, no. 13-14, pp. 3779–3784. DOI: 10.1016/J.SURFCOAT.2011.01.033.
19. Kaseem M., Fatimah S., Nashrah N., Ko Y.G. Recent progress in surface modification of metals coated by plasma electrolytic oxidation: Principle, structure, and performance. *Progress in Materials Science*, 2021, vol. 117, article number 100735. DOI: 10.1016/J.PMATSCI.2020.100735.
20. Benfedda B., Hamadou L., Benbrahim N., Kadri A., Chainet E., Charlot F. Electrochemical Impedance Investigation of Anodic Alumina Barrier Layer. *Journal of The Electrochemical Society*, 2012, vol. 159, no. 8, pp. C372–C381. DOI: 10.1149/2.068208JES.
21. Krishtal M.M., Ryumkin M.Y. Inherited chemical inhomogeneity in oxide layers deposited by the method of microarc oxidizing on hypereutectic silumins. *Metal Science and Heat Treatment*, 2007, vol. 49, no. 3-4, pp. 111–117. DOI: 10.1007/s11041-007-0021-x.
22. Siqveland L.M., Skjæveland S.M. Derivations of the Young-Laplace equation. *Capillarity*, 2021, vol. 4, no. 2, pp. 23–30. DOI: 10.46690/CAPI.2021.02.01.
23. Dilimon V.S., Shibli S.M.A. A Review on the application-focused assessment of plasma electrolytic oxidation (PEO) coatings using electrochemical impedance spectroscopy. *Advanced Engineering Materials*, 2023, vol. 25, no. 12, article number 2201796. DOI: 10.1002/ADEM.202201796.
24. Lu Xiaopeng, Chen Yan, Blawert C., Li Yan, Zhang Tao, Wang Fuhui, Kainer K.U., Zheludkevich M. Influence of SiO_2 particles on the corrosion and wear resistance of plasma electrolytic oxidation-coated AM50 Mg alloy. *Coatings*, 2018, vol. 8, no. 9, article number 306. DOI: 10.3390/COATINGS8090306.
25. Polunin A.V., Cheretaeva A.O., Borgardt E.D., Rastegaev I.A., Krishtal M.M., Katsman A.V., Yasnikov I.S. Improvement of oxide layers formed by plasma electrolytic oxidation on cast AlSi alloy by incorporating TiC nanoparticles. *Surface and Coatings Technology*, 2021, vol. 423, article number 127603. DOI: 10.1016/J.SURFCOAT.2021.127603.

СПИСОК ЛИТЕРАТУРЫ

1. Landkof B. Magnesium Applications in Aerospace and Electronic Industries // Magnesium Alloys and their Applications. 2006. P. 168–172. DOI: 10.1002/3527607552.CH28.
2. Ur Rehman Z., Choi Dongjin. Investigation of ZrO_2 nanoparticles concentration and processing time effect on the localized PEO coatings formed on AZ91 alloy // Journal of Magnesium and Alloys. 2019. Vol. 7. № 4. P. 555–565. DOI: 10.1016/J.JMA.2019.10.001.

3. Fattah-alhosseini A., Chaharmahali R., Babaei K., Nouri M., Keshavarz M.K., Kaseem M. A review of effective strides in amelioration of the biocompatibility of PEO coatings on Mg alloys // Journal of Magnesium and Alloys. 2022. Vol. 10. № 9. P. 2354–2383. DOI: 10.1016/J.JMA.2022.09.002.
4. Sedelnikova M.B., Kashin A.D., Uvarkin P.V., Tolmachev A.I., Sharkeev Y.P., Ugodchikova A.V., Luginin N.A., Bakina O.V. Porous biocoatings based on diatomite with incorporated ZrO_2 particles for biodegradable magnesium implants // Journal of Functional Biomaterials. 2023. Vol. 14. № 5. Article number 241. DOI: 10.3390/JFB14050241.
5. Xu Daokui, Han En-hau, Xu Yongbo. Effect of long-period stacking ordered phase on microstructure, mechanical property and corrosion resistance of Mg alloys: A review // Progress in Natural Science: Materials International. 2016. Vol. 26. № 2. P. 117–128. DOI: 10.1016/J.PNSC.2016.03.006.
6. Wang Guoxin, Mao Pingli, Wang Zhi, Zhou Le, Wang Feng, Liu Zheng. High strain rates deformation behavior of an as-extruded Mg-2.5Zn-4Y magnesium alloy containing LPSO phase at high temperatures // Journal of Materials Research and Technology. 2022. Vol. 21. P. 40–53. DOI: 10.1016/J.JMRT.2022.08.131.
7. Qian Yafeng, Zhao Yanhui, Dong Xiaorui, Yu Wei, Feng Jianhang, Yu Hui. Microstructure, mechanical properties and fire resistance of high strength Mg-Gd-Y-Zr alloys // Metals. 2022. Vol. 12. № 9. Article number 1456. DOI: 10.3390/MET12091456.
8. Li C.Q., Xu D.K., Zeng Z.R., Wang B.J., Sheng L.Y., Chen X.B., Han E.H. Effect of volume fraction of LPSO phases on corrosion and mechanical properties of Mg-Zn-Y alloys // Materials & Design. 2017. Vol. 121. P. 430–441. DOI: 10.1016/j.matdes.2017.02.078.
9. Cheretaeva A.O., Glukhov P.A., Shafeev M.R., Denisova A.G., Borgardt E.D., Polunin A.V., Katsman A.V., Krishtal M.M. Improvement of protective oxide layers formed by high-frequency plasma electrolytic oxidation on Mg-RE alloy with LPSO-phase // Chimica Techno Acta. 2023. Vol. 10. № 2. Article number 202310212. DOI: 10.15826/chimtech.2023.10.2.12.
10. Simchen F., Sieber M., Kopp A., Lampke T. Introduction to plasma electrolytic oxidation – an overview of the process and applications // Coatings. 2020. Vol. 10. № 7. Article number 628. DOI: 10.3390/COATINGS10070628.
11. Lu Xiaopeng, Blawert C., Huang Yuanding, Ovri H., Zheludkevich M.L., Kainer K.U. Plasma electrolytic oxidation coatings on Mg alloy with addition of SiO_2 particles // Electrochimica Acta. 2016. Vol. 187. P. 20–33. DOI: 10.1016/J.ELECTACTA.2015.11.033.
12. Mashtalyar D.V., Imshinetskiy I.M., Nadaraia K.V. et al. Effect of TiO_2 nanoparticles on the photocatalytic properties of PEO coatings on Mg alloy // Journal of Magnesium and Alloys. 2023. Vol. 11. № 2. P. 735–752. DOI: 10.1016/J.JMA.2022.10.021.
13. Bordbar-Khiabani A., Yarmand B., Mozafari M. Enhanced corrosion resistance and in-vitro biodegradation of plasma electrolytic oxidation coatings prepared on AZ91 Mg alloy using ZnO nanoparticles-incorporated electrolyte // Surface and Coatings Technology. 2019. Vol. 360. P. 153–171. DOI: 10.1016/J.SURFCOAT.2019.01.002.
14. Gnedenkov S.V., Sinebryukhov S.L., Mashtalyar D.V., Imshinetskiy I.M., Samokhin A.V., Tsvetkov Y.V. Fabrication of coatings on the surface of magnesium alloy by plasma electrolytic oxidation using ZrO_2 and SiO_2 Nanoparticles // Journal of Nanomaterials. 2015. Vol. 2015. Article number 154298. DOI: 10.1155/2015/154298.
15. Wu Jiahao, Wu Liang, Yao Wenhui, Chen Yanning, Chen Yonghua, Yuan Yuan, Wang Jingfeng, Atrens A., Pan Fusheng. Effect of electrolyte systems on plasma electrolytic oxidation coatings characteristics on LPSO Mg-Gd-Y-Zn alloy // Surface and Coatings Technology. 2023. Vol. 454. Article number 129192. DOI: 10.1016/J.SURFCOAT.2022.129192.
16. Mohedano M., Pérez P., Matykina E., Pillado B., Garcés G., Arrabal R. PEO coating with Ce-sealing for corrosion protection of LPSO Mg–Y–Zn alloy // Surface and Coatings Technology. 2020. Vol. 383. Article number 125253. DOI: 10.1016/J.SURFCOAT.2019.125253.
17. Liu Xiaohe, Liu Lei, Dong Shuai, Chen Xiao-Bo, Dong Jie. Towards dense corrosion-resistant plasma electrolytic oxidation coating on Mg-Gd-Y-Zr alloy by using ultra-high frequency pulse current // Surface and Coatings Technology. 2022. Vol. 447. Article number 128881. DOI: 10.1016/J.SURFCOAT.2022.128881.
18. Kang Min Lee, Ki Ryong Shin, Seung Namgung, Bongyoung Yoo, Dong Hyuk Shin. Electrochemical response of ZrO_2-incorporated oxide layer on AZ91 Mg alloy processed by plasma electrolytic oxidation // Surface and Coatings Technology. 2011. Vol. 205. № 13-14. P. 3779–3784. DOI: 10.1016/J.SURFCOAT.2011.01.033.
19. Kaseem M., Fatimah S., Nashrah N., Ko Y.G. Recent progress in surface modification of metals coated by plasma electrolytic oxidation: Principle, structure, and performance // Progress in Materials Science. 2021. Vol. 117. Article number 100735. DOI: 10.1016/J.PMATSCI.2020.100735.
20. Benfedda B., Hamadou L., Benbrahim N., Kadri A., Chainet E., Charlot F. Electrochemical Impedance Investigation of Anodic Alumina Barrier Layer // Journal of The Electrochemical Society. 2012. Vol. 159. № 8. P. C372–C381. DOI: 10.1149/2.068208JES.
21. Krishtal M.M., Ryumkin M.Y. Inherited chemical inhomogeneity in oxide layers deposited by the method of microarc oxidizing on hypereutectic silumins // Metal Science and Heat Treatment. 2007. Vol. 49. № 3-4. P. 111–117. DOI: 10.1007/s11041-007-0021-x.
22. Siqveland L.M., Skjaeveland S.M. Derivations of the Young-Laplace equation // Capillarity. 2021. Vol. 4. № 2. P. 23–30. DOI: 10.46690/CAPI.2021.02.01.
23. Dilimon V.S., Shibli S.M.A. A Review on the application-focused assessment of plasma electrolytic oxidation (PEO) coatings using electrochemical impedance spectroscopy // Advanced Engineering Materials. 2023. Vol. 25. № 12. Article number 2201796. DOI: 10.1002/ADEM.202201796.
24. Lu Xiaopeng, Chen Yan, Blawert C., Li Yan, Zhang Tao, Wang Fuhui, Kainer K.U., Zheludkevich M. Influence of SiO_2 particles on the corrosion and wear resistance of plasma electrolytic oxidation-coated

AM50 Mg alloy // Coatings. 2018. Vol. 8. № 9. Article number 306. DOI: 10.3390/COATINGS8090306.
25. Polunin A.V., Cheretaeva A.O., Borgardt E.D., Rastegaev I.A., Krishtal M.M., Katsman A.V., Yasnikov I.S. Improvement of oxide layers formed by plasma electrolytic oxidation on cast AlSi alloy by incorporating TiC nanoparticles // Surface and Coatings Technology. 2021. Vol. 423. Article number 127603. DOI: 10.1016/J.SURFCOAT.2021.127603.

Влияние добавки наночастиц ZrO_2 в электролит на структуру и антикоррозионные свойства оксидных слоев, формируемых плазменно-электролитическим оксидированием на сплаве $Mg_{97}Y_2Zn_1$

Полунина Алиса Олеговна*[1], научный сотрудник НИИ прогрессивных технологий
Полунин Антон Викторович[2], кандидат технических наук,
ведущий научный сотрудник НИИ прогрессивных технологий
Криштал Михаил Михайлович[3], доктор физико-математических наук, профессор,
главный научный сотрудник НИИ прогрессивных технологий
Тольяттинский государственный университет, Тольятти (Россия)

***E-mail:** **a.cheretaeva@tltsu.ru, alice_raduga@mail.ru**

[1]ORCID: https://orcid.org/0000-0002-3952-9556
[2]ORCID: https://orcid.org/0000-0001-8484-2456
[3]ORCID: https://orcid.org/0000-0001-7189-0002

Поступила в редакцию 26.06.2023 *Принята к публикации 27.10.2023*

Аннотация: Магниевые сплавы с упрочняющей длиннопериодической упорядоченной структурой (long-period stacking ordered structure, LPSO-фаза) обладают выдающими механическими свойствами, однако их низкая коррозионная стойкость обуславливает необходимость в дополнительной поверхностной защите. В работе исследовано влияние добавок в электролит наночастиц ZrO_2 в концентрации 1–4 г/л на толщину, структуру, состав, смачиваемость и антикоррозионные свойства оксидных слоев, формируемых при плазменно-электролитическом оксидировании (ПЭО) сплава $Mg_{97}Y_2Zn_1$ с LPSO-фазой. Установлено, что при ПЭО наночастицы ZrO_2 под действием электрического поля внедряются в формирующийся оксидный слой, а также снижают его пористость. Выявлено снижение количества и размеров пор вблизи барьерного слоя в местах выхода LPSO-фазы сплава к границе раздела с оксидным слоем. Малые концентрации наночастиц ZrO_2 (1–2 г/л) снижают скорость коррозии сплава по сравнению с базовым вариантом до двух раз. Минимальной плотностью тока коррозии $i_{корр}$≈14 нА/см^2 и наибольшим поляризационным сопротивлением $R_п$≈2,6 МОм·см^2 обладает образец, сформированный в электролите с добавкой 1 г/л наночастиц ZrO_2. Расчет параметров барьерной зоны оксидных слоев показал, что повышение концентрации ZrO_2 в электролите приводит к увеличению толщины барьерного слоя и росту его удельной проводимости, что отрицательно сказывается на коррозионной стойкости формируемых оксидных слоев: сопротивление барьерной зоны слоя, полученного при добавке 4 г/л ZrO_2, падает на ~20 % по сравнению с базовым вариантом (до ~1 МОм·см^2).

Ключевые слова: магниевый сплав; $Mg_{97}Y_2Zn_1$; наночастицы ZrO_2; LPSO-фаза; плазменно-электролитическое оксидирование; наночастицы; оксид циркония; краевой угол смачивания поверхности; коррозионная стойкость; проводимость барьерной зоны.

Благодарности: Работа выполнена при поддержке Российского научного фонда (проект № 21-19-00656, https://rscf.ru/project/21-19-00656/).

Статья подготовлена по материалам докладов участников XI Международной школы «Физическое материаловедение» (ШФМ-2023), Тольятти, 11–15 сентября 2023 года.

Для цитирования: Полунина А.О., Полунин А.В., Криштал М.М. Влияние добавки наночастиц ZrO_2 в электролит на структуру и антикоррозионные свойства оксидных слоев, формируемых плазменно-электролитическим оксидированием на сплаве $Mg_{97}Y_2Zn_1$ // Frontier Materials & Technologies. 2023. № 4. С. 87–98. DOI: 10.18323/2782-4039-2023-4-66-8.